Mechanism of Proton-Coupled Electron Transfer for Quinone (Q_B) Reduction in Reaction Centers of *Rb. Sphaeroides*

**M. S. Graige,**[†] **M. L. Paddock,**[†] **J. M. Bruce,**[‡] **G. Feher,**[†] **and M. Y. Okamura*,**[†]

*Contribution from the Department of Physics, 0319, University of California, San Diego,
La Jolla, California 92093-0319, and Department of Chemistry,
University of Manchester, Manchester M13 9PL, U.K.*

Received January 9, 1996[⊗]

Abstract: The mechanism of the proton-coupled electron transfer reaction, $Q_A^- Q_B^- + H^+ \rightarrow Q_A(Q_B H)^-$ (i.e. $k_{AB}^{(2)}$), was studied in reaction centers (RCs) from the photosynthetic bacterium *Rb. sphaeroides* by substituting quinones with different redox potentials into the Q_A site. These substitutions change the driving force for electron transfer without affecting proton transfer rates or proton binding equilibria around the Q_B site. The measured rate constants, $k_{AB}^{(2)}$, increased with increasing electron driving force (by a factor of 10 per 160 meV change in redox free energy). The proton-coupled electron transfer was modeled by (i) four possible two-step mechanisms in which electron transfer can precede or follow proton transfer and can be either the rate determining or fast step in the overall reaction and (ii) a one-step mechanism involving the concerted transfer of an electron and a proton. The free energy dependencies of these possible mechanisms were predicted using Marcus theory and were compared to the observed dependence. The two stepwise mechanisms in which proton transfer is rate limiting predict very different free energy dependencies from that observed. The stepwise mechanism in which rate limiting electron transfer is followed by fast proton transfer predicts a free energy dependence similar to, but significantly larger than, the observed dependence. Additional arguments are presented against this mechanism. Thus, these three two-step mechanisms are excluded by the experimental data. The best agreement with the experimental data is given by a two-step mechanism in which fast reversible proton transfer is followed by rate limiting electron transfer. For this mechanism the observed free energy dependence for $k_{AB}^{(2)}$ can be fitted using reasonable parameters of the Marcus theory. The free energy dependence predicted using a simple model for a concerted reaction also provides a reasonable fit to the data. Although the two-step mechanism (2) fits slightly better to the experimental data than the concerted mechanism, the uncertainty in the assumed parameters precludes a definitive conclusion. Thus, we propose a mechanism for proton-coupled electron transfer in native RCs (called proton-activated electron transfer) in which complete or partial protonation of the semiquinone increases the rate of the reaction by increasing the driving force for electron transfer.

Electron and proton transfer reactions are coupled in many biological energy conversion processes.[1] In the reaction centers (RC) of photosynthetic bacteria, the light induced two-electron reduction of a bound quinone molecule is coupled with uptake of 2 protons from solution in the process of creating a proton gradient across the plasma membrane.[1,2] The overall reaction for quinone reduction is given by:

$$Q_B + 2e^- + 2H^+ \rightarrow Q_B H_2 \qquad (1)$$
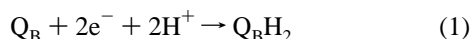
The detailed mechanism of this reduction consists of several elementary electron and proton transfer steps whose exact sequence has not been previously determined. In bacterial RCs, the main problem is that the kinetics of the second electron transfer and the first proton uptake have not been separately resolved. In this work, we separate out the two contributions to the overall observed rate by varying the redox free energy (driving force) for electron transfer while holding the free energy for the proton transfer fixed. By measuring the changes in the overall rate as a function of the redox free energy of electron transfer we tested the viability of various models to describe

proton and electron coupling observed in the RC.

The bacterial reaction center from *Rb. sphaeroides* is an integral membrane protein composed of 3 subunits (L, M, and H) and 9 cofactors: four bacteriochlorphylls, two bacteriopheophytins, two coenzyme Q_{10} molecules, and a non-heme iron atom. The cofactors are arranged along two branches, labeled A and B, shown in Figure 1. Despite the apparent two-fold symmetry, pathways for electron and proton transfer are highly asymmetric. Electron transfer proceeds from the excited primary donor, D (a bacteriochlorophyll dimer), via the bacteriochlorophyll and bacteriopheophytin in the A branch to the primary quinone, Q_A. The reduced Q_A^- then transfers an electron to the secondary quinone, Q_B. Oxidized D^+ is reduced by an electron from cytochrome c_2. A second light induced electron transfer step leads to the second electron transfer to Q_B and the uptake of 2 protons from solution.[3,4]

The electron and proton transfers to Q_B have been extensively studied by optical spectroscopy[5−8] and proton uptake
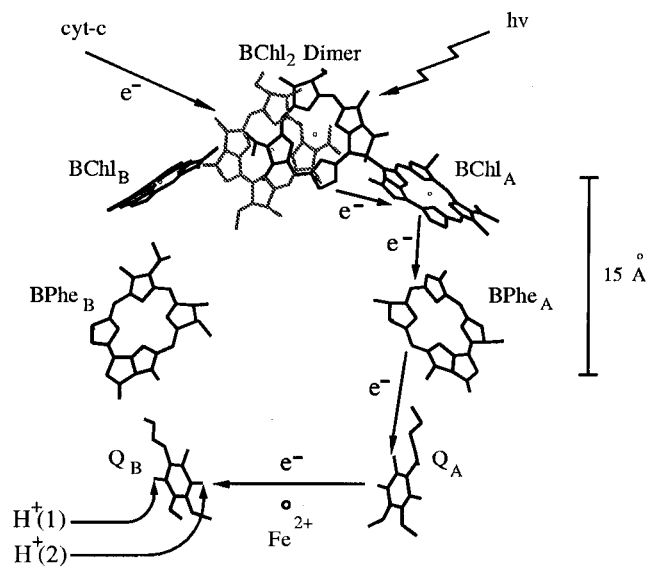

[†] University of California, San Diego.
[‡] University of Manchester.
[⊗] Abstract published in *Advance ACS Abstracts,* August 15, 1996.
(1) Cramer, W. A.; Knaff, D. B. In *Energy Transduction in Biological Membranes*; Springer-Verlag: New York, 1990.
(2) Okamura, M. Y.; Feher, G. *Annu. Rev. Biochim.* **1992,** *61,* 861−896.

(3) General review given by: Parson, W. W. In *Photosynthesis*; Amesz, J., Ed.; Elsevier: New York, 1987; pp 43−61.
(4) Feher, G.; Allen, J. P.; Okamura, M. Y.; Rees, D. C. *Nature* **1989,** *339,* 111−116.
(5) Verméglio, A.; Clayton, R. K. *Biochim. Biophys. Acta* **1977,** *461,* 159−165.
(6) Wraight, C. A. *Biochim. Biophys. Acta* **1979,** *548,* 309−327.
(7) Kleinfeld, D.; Okamura, M. Y.; Feher, G. *Biochim. Biophys. Acta* **1984,** *766,* 126−140.
(8) Kleinfeld, D.; Okamura, M. Y.; Feher, G. *Biochim. Biophys. Acta* **1985,** *809,* 291−310.

Figure 1. Arrangement of the redox cofactors in the bacterial RC.[64a] The cofactors are tightly bound and solvent inaccessible. Photon-initiated electron transfer (shown by the arrows denoted e$^-$) proceeds from a bacteriochlorophyll dimer, BChl$_2$, asymmetrically along the cofactors of the A branch, which include the monomeric bacteriochlorophyll, the bacteriopheophytin, and the primary quinone, Q$_A$. The exogenous electron donor, Cyt-c_2, donates an electron to reduce BChl$_2^+$ following its photooxidation. Q$_A^-$ serves as the electron donor to Q$_B$. Despite the apparent two-fold symmetry, the primary quinone, Q$_A$, and the secondary quinone, Q$_B$, have different properties: Q$_A$ is tightly bound and functions as a one-electron acceptor in the primary photochemistry while Q$_B$ is more weakly bound and functions as a two-electron two-proton acceptor that dissociates after reduction[29] and shuttles protons and electrons across the membrane. The first proton transfer to Q$_B$ is coupled with the second electron transfer from Q$_A^-$ to Q$_B^-$. The pathway of proton transfer to Q$_B$ deduced from mutagenesis experiments[14-20] indicates that the first proton, H$^+$(1), is bound by the carbonyl oxygen of Q$_B$ which is distal to the iron atom and the second proton, H$^+$(2), is bound by the carbonyl oxygen proximal to the iron atom. Abbreviations: BChl, bacteriochlorophyll; BPhe, bacteriopheophytin; Q, coenzyme Q$_{10}$; cyt-c, cytochrome c_2.

measurements[9-13] in native and site directed mutant[14-20] reaction centers (reviewed in refs 21 and 22). The steps involved in the proton-coupled, 2-electron reduction of Q$_B$ (called the quinone

(9) Maróti, P.; Wraight, C. A. *Biochim. Biophys. Acta* **1988**, *934*, 314−328.

(10) Maróti, P.; Wraight, C. A. *Biochim. Biophys. Acta* **1988**, *934*, 329−347.

(11) Maróti, P.; Wraight, C. A. In *Current Research in Photosynthesis*; Baltscheffsky, M., Ed.; Kluwer: Dordrecht, The Netherlands, 1990; Vol. 1, pp 1.165−1.168.

(12) McPherson, P. H.; Okamura, M. Y.; Feher, G. *Biochim. Biophys. Acta* **1988**, *934*, 348−368.

(13) McPherson, P. H.; Okamura, M. Y.; Feher, G. *Biochim. Biophys. Acta* **1993**, *1144*, 309−324.

(14) Paddock, M. L.; Rongey, S. H.; Feher, G.; Okamura, M. Y. *Proc. Natl. Acad. Sci. U.S.A.* **1989**, *86*, 6602−6606.

(15) Paddock, M. L.; Rongey, S. H.; McPherson, P. H.; Juth, A.; Feher, G.; Okamura, M. Y. *Biochemistry* **1994**, *33* (3), 734−745.

(16) Takahashi, E.; Wraight, C. A. *Biochemistry* **1991**, *31*, 855−866.

(17) Paddock, M. L.; McPherson, P. H.; Feher, G.; Okamura, M. Y. *Proc. Natl. Acad. Sci. U.S.A.* **1990**, *87*, 6803−6807.

(18) Takahashi, E.; Wraight, C. A. *Biochim. Biophys. Acta* **1992**, *1020*, 107−111.

(19) Takahashi, E.; Wraight, C. A. *Biochemistry* **1992**, *31*, 855−866.

(20) McPherson, P. H.; Schönfeld, M.; Paddock, M. L.; Okamura, M. Y.; Feher, G. *Biochemistry* **1994**, *33* (5), 1181−1193.

(21) Okamura, M. Y.; Feher, G. In *Anoxygenic Photosynthetic Bacteria*; Blankenship, R. E., Madigan, M. T., Bauer, C. E., Eds. Kluwer Academic Publishers: Dordrecht, The Netherlands, 1995; pp 577−594.

(22) Takahashi, E.; Maróti, P.; Wraight, C. A. In *Electron and Proton Transfer in Chemistry and Biology*; Diemann, E., Junge, W., Muller, Ratajezak, Hs., Eds. Elsevier: Amsterdam, Bielefeld, 1992; pp 219−236.
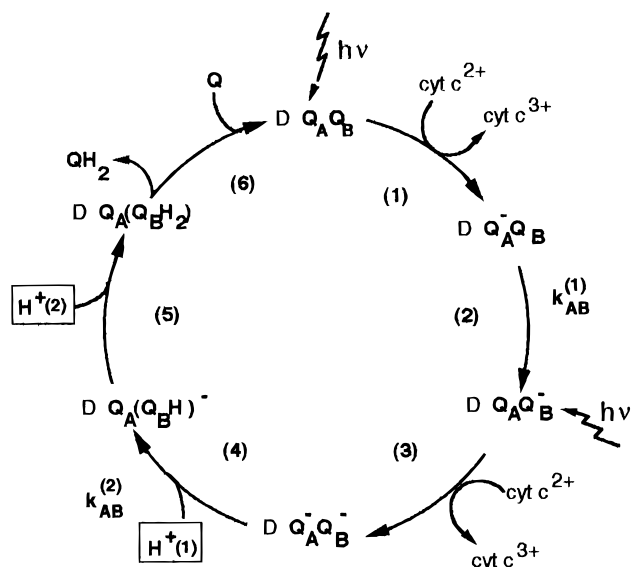
Figure 2. Quinone reduction cycle. The steps in the energy conversion process include the following: (1) absorption of a photon by a primary donor (a closely associated pair of bacteriochlorophyll molecules) followed by electron transfer to reduce Q$_A$ ($\tau \sim 200$ ps); reduction of the donor by an exogenous reducing agent, cytochrome c_2 ($\tau \sim 1$ μs), is also shown; (2) electron transfer from Q$_A^-$ to Q$_B$, $k_{AB}^{(1)}$ ($\tau \sim 100$ μs); (3) absorption of a second photon followed by electron transfer to Q$_A$ ($\tau \sim 200$ ps) and oxidation of another cytochrome c_2; (4) proton-coupled electron transfer from Q$_A^-$ to Q$_B^-$, $k_{AB}^{(2)}$ ($\tau \sim 1$ ms); (5) proton binding by the doubly reduced−singly protonated (Q$_B$H)$^-$ molecule (kinetically unresolved from the second electron transfer and the first proton transfer in native RCs); and (6) Quinone exchange.

reduction cycle) are shown in Figure 2. The two reducing equivalents for the reduction of Q$_B$ are generated at steps 1 and 3. At each step photon absorption and electron transfer produces Q$_A^-$ and oxidized cytochrome c_2. The double reduction of Q$_B$ occurs via two single electron transfer steps (2 and 4). The first electron transfer, step 2 ($k_{AB}^{(1)} \sim 10^4$ s^{-1}, pH $\sim$7.5), does not involve proton binding by Q$_B^-$ as indicated by optical,[23,24] EPR,[25] and ENDOR[26-28] measurements. The second electron transfer, step 4 ($k_{AB}^{(2)} \sim 10^3$ s^{-1}, pH $\sim$7.5), is tightly coupled with the uptake of the first proton H$^+$(1). The proton uptake and electron transfer rates measured for this step are the same.[13,14,19,20] Thus, the order of proton and electron transfer steps cannot be determined by direct measurement. The second proton, H$^+$(2), is taken up subsequent to the second electron transfer (step 5). The evidence for this comes from an analysis of electron transfer rates and proton uptake data in a site directed mutant (Glu-L212 → Gln) which blocks uptake of the second proton without changing the second electron transfer rate.[14,19,20] Exchange of dihydroquinone, Q$_B$H$_2$, for an oxidized quinone (step 6) completes the cycle.[29] In photosynthetic membranes

(23) Verméglio, A. *Biochim. Biophys. Acta* **1977**, *459*, 516−524.

(24) Land, E. J.; Simic, M.; Swallow, A. J. *Biochim. Biophys. Acta* **1971**, *226*, 239−240.

(25) Hales, B. J.; Case, E. E. *Biochim. Biophys. Acta* **1981**, *637*, 291−302.

(26) Lubitz, W.; Abresch, E. A.; Debus, R. J.; Isaacson, R. A.; Okamura, M. Y.; Feher, G. *Biochim. Biophys. Acta* **1985**, *808*, 464−469.

(27) Feher, G.; Isaacson, R. A.; Okamura, M. Y.; Lubitz, W. In *Antennas and Reaction Centers of Photosynthetic Bacteria*; Michel-Beyerle, M. E., Ed.; Springer-Verlag: Berlin, 1985; pp 174−189.

(28) O'Malley, P. J.; Chandrashekar, T. K.; Babcock, G. T. In *Antennas and Reaction Centers of Photosynthetic Bacteria*; Michel-Beyerle, M. E., Ed.; Springer-Verlag: New York, 1985; pp 339−344.

(29) McPherson, P. H.; Okamura, M. Y.; Feher, G. *Biochim. Biophys. Acta* **1990**, *1016*, 289−292.
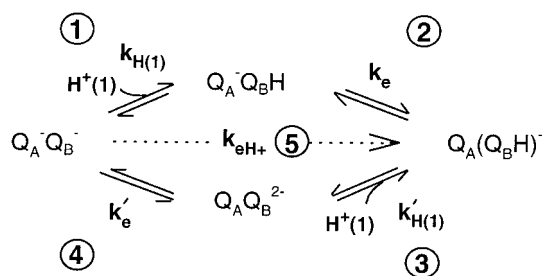
Figure 3. Possible reaction paths for the proton-coupled electron transfer reaction, $k_{AB}^{(2)}$. Along the upper path, proton transfer precedes electron transfer with formation of the protonated semiquinone intermediate. Along the lower path, electron transfer precedes proton transfer with formation of the doubly reduced dianion intermediate. Along either path, the rate limiting step could be the proton transfer (k_H, k'_H) or the electron transfer (k_e, k'_e). The circled numbers, ① − ④, denote the rate limiting step in the stepwise simplified mechanisms, 1−4, respectively, to be discussed later. The dashed line, ⑤ represents a concerted mechanism with rate constant k_{eH^+}.

the dihydroquinone is subsequently oxidized, releasing protons that contribute to an electrochemical potential across the membrane.

In this work, we examine the mechanism of coupling proton transfer with electron transfer in the $k_{AB}^{(2)}$ reaction (Figure 2, step 4). We modeled the $k_{AB}^{(2)}$ reaction in two ways. (1) The first model was as a stepwise (two-step) mechanism. In this model, the sequence of reactions giving rise to $k_{AB}^{(2)}$ can, in principle, proceed along two paths (Figure 3).[2,11] In the upper path proton transfer precedes electron transfer and a protonated semiquinone intermediate state is involved. In the lower path electron transfer precedes proton transfer and the unprotonated doubly reduced intermediate state is involved. (2) The second model was as a concerted (one-step) mechanism. In this model, transfer of an electron and a proton to Q_B^- involves only a single transition state and no intermediate states. The possibility of concerted atom and electron transfer has been proposed[30] and recent experimental evidence obtained in different chemical systems supports the idea of concerted atom (proton) and electron transfer.[31]

A direct measurement of the sequence of electron and proton transfers could unequivocally determine which of the pathways is dominant in the $k_{AB}^{(2)}$ reaction shown in Figure 3. However, as mentioned above, the observed protonation and reduction of Q_B^- occurs with the same rate.[13] We, therefore, resorted to an indirect method to investigate the reaction. This method involved the substitution of a naphthoquinone molecule with a redox potential different from that of native Q_{10} into the Q_A site, while retaining Q_{10} in the Q_B site. These constructs (called hybrid RCs) were created using procedures similar to those used previously.[32] They are based on the stronger binding of naphthoquinones to the Q_A site relative to the Q_B site.[33] The substitution should change the intrinsic rate of electron transfer k_e, k'_e, and k_{eH^+} as well as the equilibrium between the initial state and the doubly reduced intermediate state in the lower

path of Figure 3. However, since Q_B remains unchanged the proton transfer rates $k_{H(1)}$ and $k'_{H(1)}$ as well as the proton binding by Q_B^- should not change.

By substituting a series of naphthoquinone molecules into the Q_A site of RCs, the proton-coupled electron transfer rate constant, $k_{AB}^{(2)}$, was measured as a function of the driving force for electron transfer. From the dependence of the rate constant $k_{AB}^{(2)}$ on the driving force for electron transfer, several stepwise mechanisms, including any mechanism in which proton transfer is rate limiting, were ruled out.

Materials and Methods

Reagents, Buffers, and Quinones. Ethanolic solutions of ferrocene (Eastman Kodak), and diaminodurene (DAD; 2,3,5,6-tetramethyl-1,4-phenylenediamine, Aldrich) were prepared fresh prior to use. Cyt-*c* (cytochrome *c*; horse heart grade VI, Sigma) was reduced (>95%) by hydrogen gas on platinum black (Aldrich) and filtered (0.2 μM pore size acetate filter). Experiments were carried out in BMK buffer which consisted of 0.04% maltoside (dodecyl-β-D-maltoside, Anatrace), 10 mM KCl (Fisher), and 5 mM of each of the following buffers: citric acid (Calbiochem), mes (2-*N*-morpholinoethanesulfonic acid, Calbiochem), pipes (1,4-piperazine bis ethanesulfonic acid, Calbiochem), tris (2-amino-2-(hydroxymethyl)propane-1,3-diol, Fisher), ches (cyclohexylaminoethanesulfonic acid, Calbiochem), and caps (3-cyclohexylamino-1-propanesulfonic acid, Calbiochem). Solutions of ubiquinone-10 (Q_{10}, 2,3-dimethoxy-5-methyl-6-decaisoprenyl-1,4-benzoquinone, Sigma), menadione (MQ_0, 2-methyl-1,4-naphthoquinone, Sigma), and menaquinone-4 (MQ_4, 2-methyl-3-tetraisoprenyl-1,4-naphthoquinone, Sigma) were solubilized in ethanol prior to use. Trimethylnaphthoquinone (TMNQ, 2,3,5-trimethyl-1,4-naphthoquinone) and tetramethylnaphthoquinone (TEMNQ, 2,3,6,7-tetramethyl-1,4-naphthoquinone) were synthesized as described[34] and solubilized in ethanol prior to use. Terbutryne (Chem Service) and stigmatellin (Fluka) were also prepared in ethanol. All other reagents were of analytical grade.

Reaction Centers. RCs from *Rb. sphaeroides* strain R26.1 were isolated in LDAO (lauryldimethylamine *N*-oxide, Fluka) as described previously.[35] Both Q_A and Q_B were removed as described[36] by incubation in 4% LDAO, 20 mM 1,10-phenanthroline (Fisher), and 1 mM 2-mercaptoethanol (Fluka) to yield RCs with an average of 11% residual Q_A/RC and ≤1% residual Q_B/RC (as measured by 865 nm charge recombination rate and amplitude[37]). To ensure complete removal of LDAO, quinone depleted RCs were eluted from a DEAE column with a 10 mM tris/0.1% maltoside/100 mM KCl buffer, pH 7.8, then concentrated to ∼0.1 mM by centrifugation (Amicon Centricon-30) and dialyzed 1−2 days at 4 °C against BMK buffer, pH 7.2.

Electron Transfer Measurements. Absorbance changes were measured using a single beam spectrophotometer of local design.[7] Voltage output was recorded on a digital oscilloscope (Lecroy 9310M) and transferred to a PC for analysis. Actinic illumination was provided by a pulsed laser (Phase R DL2100c, 590 nm, ∼0.2 J/pulse, 0.5-μs flash width). Laser light intensity was determined to be saturating (>98%) before and after each set of experiments. Scattered laser light was blocked from reaching the PMT by using a grating monochrometer and cutoff filters. Fits to the data were made using nonlinear curve fitting software (Peakfit or Sigmaplot, Jandel) on an IBM compatible PC.

The rates of charge recombination, k_{AD} ($D^+Q_A^- \rightarrow DQ_A$), were obtained by monitoring the recovery of the primary donor (D) absorbance at 865 nm, following a saturating laser flash in RCs containing only Q_A. The charge recombination rates, k_{BD} ($D^+Q_AQ_B^- \rightarrow DQ_AQ_B$), were obtained by monitoring the slow phase of the primary

(30) (a) Perrin, C. L. *J. Phys. Chem.* **1984**, *88*, 3611−3615. (b) Zhao, X. G.; Cukier, R. I. *J. Phys. Chem.* **1995**, *99* (3), 945−954. (c) Cukier, R. I. *J. Phys. Chem.* **1994**, *98*, 2377−2381.

(31) (a) Savéant, J. M. In *Advances in Physical Organic Chemistry*; Bethel, D., Ed.; Academic Press: New York, 1990; pp 1−130. (b) Gauduel, Y.; Pommeret, S.; Antonetti, A. *J. Phys. Chem.* **1993**, *97*, 134−142. (c) Gauduel, Y.; Pommeret, S.; Migus, A.; Antonetti, A. *J. Phys. Chem.* **1991**, *95*, 533−539.

(32) Labahn, A.; Bruce, J. M.; Okamura, M. Y.; Feher, G. *Chem. Phys.* **1995**, *197*, 355−366.

(33) Gunner M. R.; Tiede, D. M.; Prince, R. C.; Dutton, P. L. In *Functions of Quinones in Energy Conserving Systems*; Trumpower, B. L., Ed.; Academic Press: New York, 1982; pp 265−269.

(34) Mashraqui, S.; Keehn, P. *Synth. Commun.* **1982**, *12*, 637.

(35) Paddock, M. L.; Rongey, S. H.; Abresch, E. C.; Feher, G.; Okamura, M. Y. *Photosynth. Res.* **1988**, *17*, 75−96.

(36) Okamura, M. Y.; Isaacson, R. A.; Feher, G. *Proc. Natl. Acad. Sci. U.S.A.* **1975**, *72*, 3491−3495.

(37) Okamura, M. Y.; Debus, R. J.; Kleinfeld, D.; Feher, G. In *Functions of Quinones in Energy Conserving Systems*; Trumpower, B. L., Ed.; Academic Press: New York, 1982; pp 299−317.

donor recovery, following a laser flash, in RCs with both Q_A and Q_B binding sites occupied. The occupancy of the Q_B site was determined from the relative amplitudes of the two kinetic phases of charge recombination.[37] Rate constants for $k_{AB}^{(2)}$ (step 4, Figure 2) were determined by monitoring the decay of semiquinone absorbance at wavelengths between 400 and 500 nm following a second laser flash in RC solutions containing an exogenous reductant to reduce the oxidized primary donor, D^+. To avoid interference with the $k_{AB}^{(2)}$ kinetics the identity and concentration of exogenous reductant was varied. Below pH 9, DAD ($\sim$100 μM) was used. Above pH 9, three different exogenous reductants—DAD, cyt-c ($\sim$30 μM), and ferrocene ($\sim$60 μM)—were used (separately) to reduce D^+; they gave similar results. The kinetics of reduction of D^+ by DAD following the second laser flash were recorded on a second digital oscilloscope in order to better quantitate and deconvolve this rate ($\tau \sim$ 50 to 80 ms) from the $k_{AB}^{(2)}$ rate. It was noted that the rate constant $k_{AB}^{(2)}$ was not dependent on the identity of the exogenous reductant nor was it sensitive to changes in the concentration of maltoside between 0.01% and 0.1% (w/v) or ionic strength between 10 mM and 60 mM KCl. The triazine herbicide, terbutryne, blocks electron transfer to Q_B.[38] Consequently, comparison of the flash induced kinetics before and after the addition of 100 μM terbutryne allowed the identification of kinetics associated with Q_B reduction.

pH Measurements. pH measurements were performed with a Cole-Palmer Chemcadet research pH meter equipped with an Ingold No. ES18726 pH electrode calibrated with standards that spanned the measured pH values.

Reconstitution of the Q_A Binding Site. Naphthoquinone (NQ) was added in ethanolic solution by a micropipet to a conical reaction vial and dried by evaporation, leaving a film of quinone on the glass surface. The quantity of the naphthoquinone added was determined by its solubility in buffer solution and the amount expected to be bound in the Q_A site at equilibrium. Solubilities in BMK buffer for Q_{10}, MQ_0, MQ_4, TMNQ, and TEMNQ were approximately 1, 30, 25, 23, and 14 μM, respectively, at room temperature. Quinone depleted RCs in BMK buffer were added to the reaction vial and the RCs were incubated (32 °C, $\sim$30 min with stirring) to yield RCs with full Q_A site occupancy and activity.

Reconstitution of the Q_B Binding Site. Reaction kinetics are sensitive to detergent type and concentration.[8,13] Therefore, a method to incorporate Q_{10} into the Q_B binding site without changing the buffer or detergent conditions was developed. Q_{10} was added in ethanolic solution by a micropipet to $\sim$1 mg of Celite (diatomacious earth, Fisher). After evaporation of the ethanol, the dry Celite/Q_{10} powder was added to 1 mL of RC sample in which Q_A was previously reconstituted. This sample was incubated for $\sim$20 min (high pH samples, pH >9, required longer incubation times, ca. 1–2 h) at 25 °C with stirring. An occupancy of the Q_B site between 75% and 90% was achieved at pH 7.2. It was sometimes necessary to repeat the Celite step in order to fully populate the Q_B site. Since the solubility of Q_{10} in BMK buffer is very low ($\leq$1 μM), the rate of Q_{10} incorporation into the Q_B binding site by other methods (which do not involve the addition of detergent) is significantly slower. It is hypothesized that Q_{10} can associate with Celite, effectively increasing the surface area on which the RC and Q_{10} can interact thereby facilitating more rapid incorporation.

During the incubation period, an equilibrium in the Q_A site between Q_{10} and NQ was established that depended on the concentrations of the quinones and their binding affinities at the Q_A and Q_B sites. The quantity of Q_{10} added to the Celite was optimized to maximize the fraction of RCs which had a naphthoquinone in the Q_A site (usually 40% to 60% of the RC population, depending on the individual NQ binding constant and solubility) and Q_{10} in the Q_B site.

Native RCs ($Q_{10(A)}$ $Q_{10(B)}$), used as controls, were prepared by the same procedure as hybrid RCs ($NQ_{(A)}$ $Q_{10(B)}$). The rates observed in native RCs were the same as those observed in RCs prior to quinone removal and reconstitution.

(38) (a) Stein, R. R.; Castellvi, A. L.; Bogacz, J. P.; Wraight, C. A. In *Biosynthesis of the Photosynthetic Appratus*: *Molecular Development, and Regulation*; Hallick, R., Staehlin, L. A., Thornber, J. P., Eds.; Alan R. Liss: New York, 1984; pp 167–183. (b) Okamura, M. Y. ref 38a, pp 381–390.

Results

Naphthoquinone in the Q_A Site of RCs; Q_B Site Unoccupied/Inactive. RCs containing naphthoquinone, NQ, in the Q_A site were prepared by incubating inactive RCs (from which the native Q_{10} had been removed) in buffer containing NQ. The amplitude of the kinetic signal

$$D\,NQ \underset{k_{AD}}{\overset{h\nu}{\rightleftharpoons}} D^+NQ^-$$
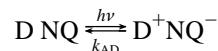
monitored at 865 nm following a saturating laser flash (on the time scale of $k_{AD} \sim$10 s^{-1}) was used to monitor the activity of the reconstituted RCs. It increased during incubation reaching a limiting value of 85% bleaching of the donor exciton band, as expected for a fully occupied Q_A site. The rate of charge recombination ($D^+Q_A^- \rightarrow DQ_A$ k_{AD}) showed either that the NQ was not incorporated into the Q_B site or that it was inactive in the Q_B site.[39] Characteristic rate constants, k_{AD}, for different NQs were measured and are shown in Table 1.

The semiquinone anion spectra of NQ^- and Q_{10}^- in the Q_A site was measured after a single saturating laser flash (measured in RCs with only Q_A present and in the presence of exogenous electron donor, DAD, to reduce D^+). The absorptions of NQ^- and Q_{10}^- (Figure 4) at 450 nm are approximately the same. However, NQ^- has a much greater absorbance in the region from $\sim$470 to 490 nm. This difference in spectra offers the possibility to specifically monitor the $NQ^- \rightarrow NQ$ reactions in hybrid RCs (i.e., $DNQ_A^-Q_{10(B)}^- + H^+ \rightarrow DNQ_A(Q_{10(B)}H)^-$ ($k_{AB}^{(2)}$)) in this wavelength region.
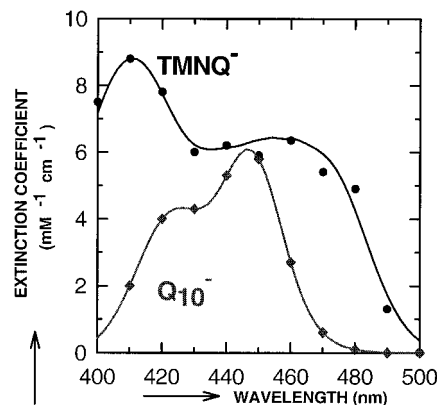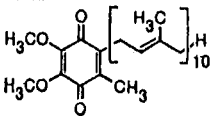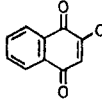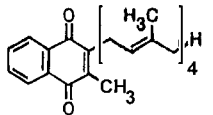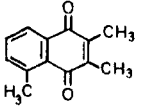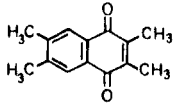

Figure 4. Semiquinone anion spectra for Q_{10}^- and TMNQ$^-$ in the Q_A site of RCs determined from the optical absorbance change after a single saturating laser flash in the presence of the exogenous electron donor, DAD, which reduces D^+. DAD was chosen for its negligible absorption in this wavelength region.[23] Since the absorbance of neutral quinone is also negligible in this region, the measured changes depend only on the extinction coefficients of the quinone anion in the reaction DQ_A + $DAD_{red.} \rightarrow DQ_A^-$ + $DAD_{ox.}$ ($h\nu$). The Q_{10}^- spectrum was determined in RCs having 0.7 Q_{10}/RC. The TMNQ$^-$ spectrum (0.95 TMNQ/RC) was corrected for the residual Q_{10} in the Q_A site. Note: The spectrum of TMNQ$^-$ is representative of naphthoquinone (NQ$^-$) spectra in general. The lines though the Q_{10}^- and TMNQ$^-$ data points represent the best fits of 3 and 4 Gaussian waveforms, respectively. (Conditions: 3 μM RCs, 100 μM DAD, 5 mM BMK buffer, pH 7.2, $T = 23$ °C. Spectrometer bandwidth was 10 nm.)

Hybrid RCs ($NQ_{(A)}$ $Q_{10(B)}$). To prepare hybrid RCs containing naphthoquinone in the Q_A site and ubiquinone in the Q_B site, the Q_A binding site reconstitution was followed by incubation in the presence of Q_{10}. The amplitude of the kinetic signal remained the same after incubation, but the rate of the

(39) This observation was elaborated on previously by: Giangiacomo, K. M.; Dutton, P. L. *Proc. Natl. Acad. Sci. U.S.A.* **1989**, *86*, 2658–2662.

Table 1. Electron Transfer Kinetics in Hybrid and Native RCs[a]

| RC type	Q_A structure	k_{AD} (s⁻¹)	k_{BD} (s⁻¹)	relative *in situ* redox potential[b]	$k_{AB}^{(2)}$ (s⁻¹)[d]	relative $k_{AB}^{(2)}$
$Q_{10(A)},Q_{10(B)}$		7.9 ± 0.4	0.69 ± 0.03	0 meV (defined)	2720 ± 50	1 (defined)
$MQ_{0(A)},Q_{10(B)}$		7.2 ± 0.3	1.15 ± 0.12	15 ± 5 meV	2360 ± 70	0.88 ± 0.05
$MQ_{4(A)},Q_{10(B)}$		13.5 ± 0.5	0.32 ± 0.06	-46 ± 9meV	7300 ± 400	2.7 ± 0.3
$TMNQ_{(A)},Q_{10(B)}$		13.3 ± 0.5	0.15 ± 0.02	-95 meV [c]	12900 ± 400	4.7 ± 0.4
$TEMNQ_{(A)},Q_{10(B)}$		21.1 ± 0.6	0.15 ± 0.02	-120 ± 10 meV	16700 ± 700	6.1 ± 0.4

[a] Experimental uncertainties represent one standard deviation of the mean of at least 4 measurements. Q_{10} = ubiquinone-10, MQ_0 = 2-methyl-1,4-naphthoquinone, MQ_4 = 2-methyl-3-tetraisoprenyl-1,4-naphthoquinone, TMNQ = 2,3,5-trimethyl-1,4-naphthoquinone, and TEMNQ = 2,3,6,7-tetramethyl-1,4-naphthoquinone. The Q_B site occupancy by native Q_{10} was at least 80% for all measurements (except k_{AD}). (Conditions: 14 μM RCs, 5 mM BMK buffer, pH 7.2, T = 23 °C.) [b] These values were determined using one of the methods described in the text. [c] Published value of ref 42. [d] Data for hybrid RCs obtained from measurements made at 450 and 485 nm as described in the text.

recombination became characteristic of charge recombination in RCs having both the Q_A and Q_B sites occupied. The presence of hybrid RCs was confirmed by the characteristically slower recombination kinetics (k_{BD}) in hybrid RCs compared to those in native RCs. The rate of charge recombination in hybrid RCs containing low potential quinones, $D^+NQ_{(A)}^-Q_{10(B)}^- \rightarrow DNQ_{(A)}Q_{10(B)}$, is typically slower than the rate of recombination in native RCs, ($D^+Q_{10(A)}^-Q_{10(B)}^- \rightarrow DQ_{10(A)}Q_{10(B)}$), due to a slower indirect recombination[32] (see Table 1).

Due to the competition between Q_{10} and NQ for the Q_A binding site, only a fraction of the Q_A binding sites were occupied by a NQ molecule. The equilibrium fraction of hybrid RCs/total RCs was a function of the amount of NQ and Q_{10} added to the solution, their solubilities, and their relative binding affinities. To interpret the observed $k_{AB}^{(2)}$ kinetics it was necessary to measure the fraction of hybrid RCs in a sample. This was accomplished by two different procedures.

(**1**) The first method was based on the difference in recombination rates, k_{BD}, for native and hybrid RCs. As mentioned above, hybrid RCs containing low potential quinones recombine slower than native RCs.[32] Consequently, two phases of charge recombination, k_{BD}*native* ($D^+Q_{10(A)}^-Q_{10(B)}^- \rightarrow DQ_{10(A)}Q_{10(B)}$) and k_{BD}*hybrid* ($D^+NQ_{(A)}^-Q_{10(B)}^- \rightarrow DNQ_{(A)}Q_{10(B)}$), were observed in RC samples incubated in the presence of NQ and Q_{10}. One phase had a rate identical to recombination in native RCs; the other phase had a rate slower than native RC recombination. The fraction of hybrid RCs, f, was determined from the amplitudes of the two phases, i.e., f = (amplitude k_{BD}*hybrid*)/(amplitude k_{BD}*hybrid* + amplitude k_{BD}*native*). Using this method, the fraction of hybrid RCs calculated for samples containing MQ_4, TMNQ, or TEMNQ was 0.60 ± 0.03, 0.49 ± 0.07, and 0.49 ± 0.03, respectively.

(**2**) The second method utilized the difference between the semiquinone anion absorption spectra of NQ^- and Q_{10}^- (see Figure 4). This procedure was especially useful for characterizing samples containing naphthoquinones with potentials near Q_{10}, for which recombination kinetics are similar to those in native RCs. The change in optical absorption after a single saturating laser flash was measured in samples containing native and hybrid RCs in the presence of the exogenous reductant, ferrocene, to reduce D^+, and stigmatellin, a potent inhibitor of electron transfer from Q_A^- to Q_B.[40] Ferrocene reduces D^+ on a rapid time scale compared to the recombination reaction, k_{AD}, thus the reactions following a laser flash are

$$DNQ_A + Fe^{2+} \xrightarrow{h\nu} DNQ_A^- + Fe^{3+}$$

$$DQ_{10(A)} + Fe^{2+} \xrightarrow{h\nu} DQ_{10(A)}^- + Fe^{3+}$$
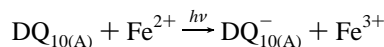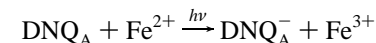
where Fe is the exogenous reductant. Measurements were made at 410 nm, the wavelength at which the difference between NQ_A^- and Q_{10}^- extinctions is greatest (see Figure 4) and where ferrocene, the exogenous reductant, has a negligible absorbance change ($\sim$3% of the signal). The fraction of hybrid RCs was calculated from the observed change in absorbance following the laser flash, ΔA^{obs}, the measured extinction coefficients, $\Delta\epsilon_{NQ_{(A)}}^{410nm}$ = 8.8 mM⁻¹ cm⁻¹ and $\Delta\epsilon_{Q_{10(A)}}^{410nm}$ = 2.0 mM⁻¹ cm⁻¹ ± 10%, and the concentration of reaction centers, [RC], as

(40) (a) Bibikov, S. I.; Bloch, D. A.; Cherepanov, D. A.; Oesterhelt, D.; Semenov, A. Y. *FEBS Lett.* **1994**, *341*, 10−14. (b) Lancaster, C. R. D.; Michel, H. In *Reaction Centers of Photosynthetic Bacteria. Structure and Dynamics*; Michel-Beyerle, M. E., Ed.; Springer-Verlag: New York, 1996; pp 1−13. (c) Stigmatellin has been observed in this work to inhibit electron transfer between Q_A and Q_B in native RCs when added in an approximately stoichiometric amount.

$f = (\Delta A^{obs} - \Delta\epsilon_{Q_{10(A)}^{-}}^{410nm}[RC])/\{(\Delta\epsilon_{NQ_{(A)}^{-}}^{410nm} - \Delta\epsilon_{Q_{10(A)}^{-}}^{410nm})[RC]\}$. The fraction of hybrid RCs, calculated by the semiquinone anion absorption method, for samples containing MQ_0, MQ_4, TMNQ, or TEMNQ was 0.34 ± 0.08, 0.52 ± 0.04, 0.40 ± 0.02, and 0.45 ± 0.03, respectively. The two experimental methods gave similar values for the fraction of hybrid RCs. These values are in fair agreement with calculated values based on binding constants published in the literature for naphthoquinone and ubiquinone molecules in the Q_A and Q_B sites.[41] Assuming naphthoquinone and ubiquinone are present at their solubility limit and $[RC] = 10\ \mu M$, equilibrium values of 0.38, 0.81, 0.49, and 0.48 are calculated for samples containing MQ_0, MQ_4, TMNQ, and TEMNQ, respectively.

Determination of $k_{AB}^{(2)}$ in Hybrid and Native RCs. The rate constant for the proton-coupled second electron transfer, $k_{AB}^{(2)}$, was measured in hybrid and native RCs by monitoring the absorbance change at 485 nm following a second laser flash in the presence of the exogenous reductant, DAD, to reduce D^+. Native RCs showed no change in absorbance following the second laser flash (Figure 5a) as expected from the negligibly small extinction coefficient of Q_{10}^{-} at 485 nm (see Figure 4). However, the RC sample incubated in NQ and Q_{10} (i.e. containing both native and hybrid RCs) exhibited a transient which was attributed to electron transfer from NQ^- in hybrid RCs ($NQ_{(A)}^{-}\ Q_{10(B)}^{-} + H^+ \rightarrow NQ_{(A)}\ (Q_{10(B)}H)^-$). For example, RCs containing TMNQ show a decay at 485 nm with a characteristic time of 0.68 ms (Figure 5b).

For comparison, $k_{AB}^{(2)}$ was also measured in native RCs by monitoring the semiquinone decay at 450 nm after a second laser flash (Figure 5c). The 2.8-ms decay, due to the transfer from Q_{10}^{-} in native RCs ($Q_{10(A)}^{-}\ Q_{10(B)}^{-} + H^+ \rightarrow Q_{10(A)}\ (Q_{10(B)}H)^-$), is in agreement with previous results[13] and is slower than in hybrid RCs. At 450 nm, the electron transfer rates from both $NQ_{(A)}^{-}$ and $Q_{10(A)}^{-}$ to $Q_{10(B)}^{-}$ were measured simultaneously in the same sample by monitoring semiquinone decay following two laser flashes in a RC sample that contained both native and hybrid RCs. A biphasic decay was observed that could be fitted with two decay times, one corresponding to the decay time of native RCs ($Q_{10(A)}^{-}\ Q_{10(B)}^{-} + H^+ \rightarrow Q_{10(A)}\ (Q_{10(B)}H)^-$) and one corresponding to hybrid RCs ($NQ_{(A)}^{-}\ Q_{10(B)}^{-} + H^+ \rightarrow NQ_{(A)}\ (Q_{10(B)}H)^-$). For example, the biphasic decay shown in Figure 5d could be fitted with the time constants of 0.68 ms (measured at 485 nm for hybrid RCs) and 2.8 ms (measured at 450 nm for native RCs). Values of the rate constant $k_{AB}^{(2)}$ with various naphthoquinones in the Q_A site were measured and are summarized in Table 1.

***In Situ* Redox Potentials of NQs.** The *in situ* redox potentials of the different naphthoquinones in the Q_A site were determined by three different methods.

(1) The first method used delayed fluorescence. This method was applied to determine the redox potential of TMNQ relative to Q_{10} in the Q_A site.[42] A value of $E_M(TMNQ) - E_M(Q_{10}) = -95$ meV has been previously reported.[42,43]

**(2)** The second method was based on the charge recombination, k_{AD}. An empirical relation between the *in situ* redox potential and the rate of recombination, k_{AD}, was applied to

(41) Warncke, K.; Gunner, M. R.; Braun, B. S.; Gu, L.; Yu, C.; Bruce, J. M.; Dutton, P. L. *Biochemistry* **1994**, *33*, 7830−7841.

(42) Woodbury, N. W.; Parson, W. W.; Gunner, M. R.; Prince, R. C.; Dutton, P. L. *Biochim. Biophys. Acta* **1986**, *851*, 6−22.

(43) Gunner, M. R.; Dutton, P. L. *J Am. Chem. Soc.* **1989**, *111*, 3400−3412.

(44) For a complete discussion of this point see: Feher, G.; Arno, T. R.; Okamura, M. Y. In *The Photosynthetic Bacterial Reaction Center*; Breton, J., Verméglio, A., Eds.; Plenum Publishing: New York, 1988; pp 271−287.
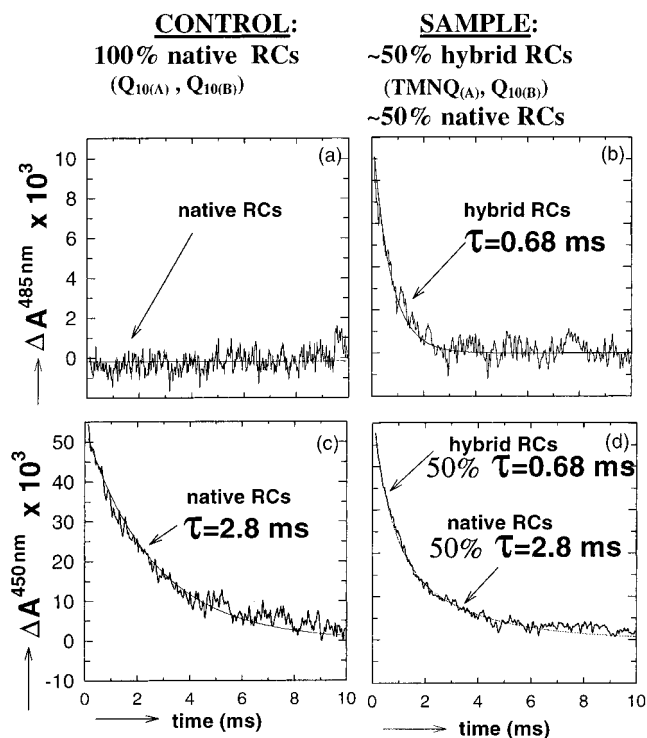
Figure 5. Optical kinetics data for the second electron transfer rate constant, $k_{AB}^{(2)}$. (a) Change in optical absorption monitored at 485 nm in native ($Q_{10(A)}$, $Q_{10(B)}$) RCs. Note the lack of change in absorption following a second laser flash. (b) Change in optical absorption monitored at 485 nm for a sample containing both hybrid (TMNQ$_{(A)}$, $Q_{10(B)}$) and native ($Q_{10(A)}$, $Q_{10(B)}$) RCs (~50:50 mix). The observed change in optical absorption is due exclusively to electron transfer in hybrid RCs since only the decay of naphthoquinone anion absorbance can be observed at this wavelength (see also Figure 4). (c) Change in optical absorption monitored at 450 nm for native RCs. (d) Change in optical absorption monitored at 450 nm for a sample containing both hybrid (TMNQ$_{(A)}$, $Q_{10(B)}$) and native ($Q_{10(A)}$, $Q_{10(B)}$) RCs. The decay is biphasic with one phase due to semiquinone decay in hybrid RCs and the other due to semiquinone decay in native RCs. Solid lines represent exponential fits to the data. The kinetics of the primary donor re-reduction by DAD ($k_{DAD} \sim 20\ s^{-1}$) have been subtracted for clarity. Addition of terbutryne to inhibit electron transfer to Q_B eliminated the kinetic phases shown in b, c, and d. (Conditions: 14 μM RC, 100 μM DAD, 5 mM BMK buffer, pH 8.8, $T = 23$ °C. Spectral bandwidth was 2.3 nm.)

determine the redox potential of TEMNQ in the Q_A site. The empirical relation[43] (at pH 7.3, $k_BT = 25$ meV) (eq 2)

$$E_M(NQ) - E_M(Q_{10}) = -56.6 \log(k_{AD} - 7.0) - 53.3\ \text{meV} \tag{2}$$

is based on an observed correlation between the redox potential measured by delayed fluorescence and the recombination rate, k_{AD}. A value of $E_M(TEMNQ) - E_M(Q_{10}) = -120$ meV was calculated from eq 2 using the observed value, $k_{AD} = 21.1\ s^{-1}$. Equation 2 can be used to obtain fairly accurate estimates of the relative *in situ* redox potential for quinones with low potential $[E_M(NQ) - E_M(Q_{10}) \lesssim -80$ meV] for which delayed fluorescence has not been measured. The rate constant, k_{AD}, becomes much less sensitive to changes in the redox potential of Q_A as the relative redox potential becomes greater than ca. -80 meV.[44] Thus, the redox potentials of MQ_0 and MQ_4 $[E_M(NQ) - E_M(Q_{10}) \gtrsim -80$ meV] were estimated using an alternate method described in the next section.

(3) The third method was based on the charge recombination, k_{BD}. It was applied to measure the *in situ* redox potentials of MQ_0 and MQ_4. Charge recombination from the state

$D^+Q_AQ_B^-$ has two components; one is the direct recombination from Q_B^- to D^+ ($k_{direct} = 0.12$ s^{-1} at pH 7.3)[32] and the other is an indirect recombination through the state $D^+Q_A^-Q_B$.

From the indirect rate the energy difference between the states $D^+Q_A^-Q_B$ and $D^+Q_AQ_B^-$ can be obtained. Since the energy of the $D^+Q_AQ_B^-$ state is unaffected by the quinone substitution at the Q_A site, the change in the energy difference is equal to the relative *in situ* redox potential of the naphthoquinone. The energy difference between the states $D^+Q_A^-Q_B$ and $D^+Q_AQ_B^-$ can be obtained as follows. The states $D^+Q_AQ_B^-$ and $D^+Q_A^-Q_B$ are in dynamic equilibrium with the population of each determined by the Boltzmann distribution

$$\alpha = \frac{1}{\exp\{-[\Delta G^0_{AB}/k_BT]\}-1} \qquad (3)$$

where α is the mole fraction of RCs in the state $D^+Q_A^-Q_B$ and ΔG^0_{AB} is the standard free energy between the states. The observed rate is a sum of the direct and indirect recombination rates.[7,45]

$$k_{obs.} = k_{direct} + k_{indirect} = (1 - \alpha)k_{direct} + \alpha k_{AD} \qquad (4)$$

The experimentally determined values of $k_{obs.}$, k_{AD}, and k_{direct} were used in eqs 3 and 4 to calculate the free energy, ΔG^0_{AB}, between states for RCs with MQ$_0$ or MQ$_4$ in the Q_A site. The relative *in situ* redox potentials of MQ$_0$ and MQ$_4$ were obtained by subtracting the energy difference observed in native RCs (-60 meV) from the calculated ΔG^0_{AB}. Thus, this method provides a sensitive measure of the relative *in situ* redox potential for quinones with potentials which are not greatly shifted from that of native Q_{10}; this method is not applicable to quinones with potentials shifted more than ca. -80 meV since for these quinones the mechanism of recombination becomes predominantly direct. The relative *in situ* redox potentials of MQ$_0$ and MQ$_4$ were calculated as $+15$ and -46 meV, respectively. Uncertainties were estimated from the errors associated with the determination of $k_{obs.}$, k_{AD}, and k_{direct}. The rates and relative redox potentials for all quinones are summarized in Table 1.

pH Dependence of $k^{(2)}_{AB}$. The pH dependence of $k^{(2)}_{AB}$ in native and hybrid RCs containing TMNQ was measured and is shown in Figure 6. The rate decreases $\sim$0.3 decades/pH unit between pH 5 and 8 and almost a full decade/pH unit for pH $>$9.[6,8,46] The shape of the curve for hybrid RCs appears to be the same as for native. An approximately constant 4.5-fold increase in $k^{(2)}_{AB}$ for hybrid RCs was observed over the pH range from 4.5 to 9.5. This indicates that the same mechanism for $k^{(2)}_{AB}$ operates over this pH range in hybrid and native RCs.

Discussion

To test the mechanism of the proton-coupled second electron transfer reaction $Q_A^-Q_B^- + H^+ \rightarrow Q_A(Q_BH)^-$ ($k^{(2)}_{AB}$) in bacterial RCs, naphthoquinone molecules with redox potentials different from that of the native Q_{10} were substituted into the Q_A binding site while retaining Q_{10} in the Q_B site. The substitutions in the Q_A site change the free energy for the electron transfer reaction (and thereby change the electron transfer rates and equilibrium) but they do not have an effect on proton transfer rates or proton binding equilibria at the Q_B site. Consequently, from the
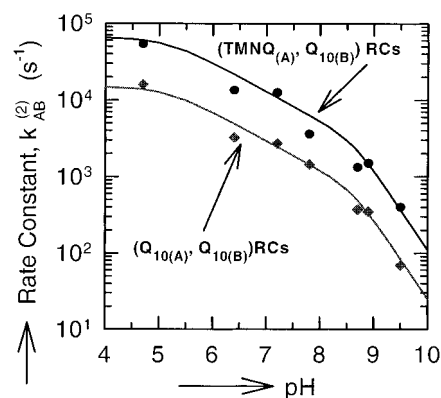
Figure 6. pH dependence of the proton-coupled electron transfer rate constant, $k^{(2)}_{AB}$, for native RCs (♦) determined from the decay of semiquinone absorbance at 450 nm and for hybrid RCs (●) determined from the decay of semiquinone absorbance at 450 and 485 nm as described in the text. The shape of the curve has previously been determined.[6,8,46] The line through the native data represents a least-squares fit of the curve to the data observed in this work. The fitted line through the hybrid RC data represents an approximately 4.5-fold increase over the native rate at all pH. The pH of the buffer was adjusted prior to the addition of RCs. Statistical uncertainty, representing one standard deviation of the mean, was within the radius of the dot for data points at pH 4.7, 7.2, 9.0, and 9.5. Data at other pHs were single measurements. Uncertainty in pH was $\pm$0.05 pH units. (Conditions: 7$-$14 μM RC, 50$-$100 μM DAD, 5 mM BMK buffer, $T = 23$ °C.)

experimentally observed dependence of $k^{(2)}_{AB}$ on the free energy for electron transfer, information about the mechanism and energetics of this reaction was obtained.

Free Energy Dependence of the Electron Transfer Rate. To predict the free energy dependence of $k^{(2)}_{AB}$ for the different reaction mechanisms shown in Figure 3, we discuss first the dependence of the electron transfer rate on the redox free energy for electron transfer (driving force). The rate of electron transfer according to Marcus theory is given by

$$k_{et} = \frac{2\pi|T_{AB}|^2}{\hbar(4\pi\lambda k_BT)^{1/2}} \exp\left\{-\left[\frac{(\Delta G^0_{et} + \lambda)^2}{4\lambda k_BT}\right]\right\} \qquad (5)$$

where ΔG^0_{et} is the free energy for electron transfer (defined as the energy of the final minus the initial state), λ is the reorganization energy, and T_{AB} is the tunneling matrix element.[47] To graphically illustrate the free energy dependence of the rate, a normalized rate constant, k_{et}, is plotted on a log scale vs ΔG^0_{et} (Figure 7). The function is parabolic. The slope of the free energy dependence varies with ΔG^0_{et} and can be used to characterize an electron transfer reaction.

A slope describing the dependence of $k^{(2)}_{AB}$ on the free energy for electron transfer (characteristic of the reaction mechanism in RCs) can be obtained from the results of the quinone substitution experiments. The free energy for electron transfer in hybrid RCs (NQ$_{(A)}$ Q$_{10(B)}$), ΔG^0_{Hybrid}, is given by

$$\Delta G^0_{Hybrid} = \Delta G^0_{k_{AB}^{(2)}} + \delta\Delta G^0 \qquad (6)$$

where $\Delta G^0_{k_{AB}^{(2)}}$ is the free energy of electron transfer in native RCs (Q$_{10(A)}$ Q$_{10(B)}$), and $\delta\Delta G^0$ is the difference in the *in situ* redox free energy of NQ$^-$/NQ compared to that of Q$_{10}^-$/Q$_{10}$

(45) Wraight, C. A.; Stein, R. R. *FEBS Lett.* **1980**, *113*, 73$-$77.
(46) Verméglio, A. In *Functions of Quinones in Energy Conserving Systems*; Trumpower, B. L., Ed.; Academic Press: New York, 1982; pp 169$-$180.

(47) (a) Marcus, R. A. *J. Chem. Phys.* **1956**, *24*, 966$-$978. (b) Marcus, R. A.; Sutin, N. *Biochim. Biophys. Acta* **1985**, *811*, 265$-$322. (c) Reviewed by: Albery, J. W. *Annu. Rev. Phys. Chem.* **1980**, *31*, 227$-$263. (d) Reviewed by: Yates, K. *J. Phys. Org. Chem.* **1989**, *2*, 300$-$322.
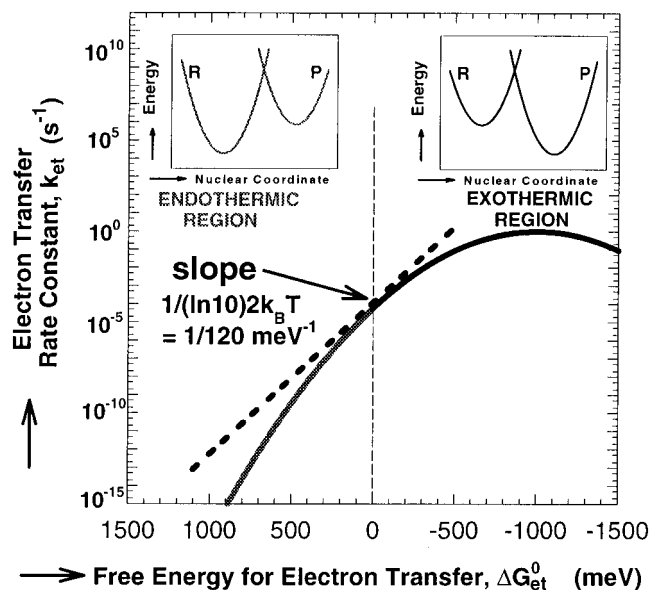
Figure 7. Dependence of the electron transfer rate constant on ΔG_{et}^0 predicted by the Marcus theory (eq 5). A slope less than $1/(2(\ln 10)k_BT)$ indicates an exothermic reaction ($\Delta G_{et}^0 < 0$) while a slope greater than $1/(2(\ln 10)k_BT)$ indicates an endothermic electron transfer reaction ($\Delta G_{et}^0 > 0$). The reorganization energy, λ, was arbitrarily chosen to be 1.0 eV. Insets show the potential energy vs nuclear coordinate for endothermic and exothermic electron transfer reactions. The curves labeled R represent the potential energy of the entire system: donor, acceptor, and surrounding before electron transfer from the reduced donor to the acceptor. The curves labeled P represent the potential energy of the entire system after the electron transfer has occurred.

(Table 1, column 5). We assume that the values of λ and T_{AB} remain the same upon NQ substitution into the Q_A site, i.e., only the free energy for electron transfer is changed. Therefore, the free energy dependence of the (relative) rate can be obtained from eqs 5 and 6. For $\delta\Delta G^0 \ll \lambda$, $\Delta G_{k_{AB}^{(2)}}^0$, the log of the ratio of the rate constants in hybrid RCs to the rate in native RCs is given by:

$$\log \frac{k_{AB}^{(2)} hybrid}{k_{AB}^{(2)} native} = -\frac{\delta\Delta G^0}{2(\ln 10)k_BT}\left(1 + \frac{\Delta G_{k_{AB}^{(2)}}^0}{\lambda}\right) \quad (7)$$

Thus, for small $\delta\Delta G^0$, the log of the ratio of rates is linearly dependent on the change in the driving force, $\delta\Delta G^0$. The derivative of eq 7 with respect to $\delta\Delta G^0$ yields the slope of the free energy dependence:

$$\frac{\partial\left(\log\dfrac{k_{AB}^{(2)} hybrid}{k_{AB}^{(2)} native}\right)}{\partial(\delta\Delta G^0)_\lambda} = \frac{1}{2(\ln 10)k_BT}\left(1 + \frac{\Delta G_{k_{AB}^{(2)}}^0}{\lambda}\right) \quad (8)$$

Equation 8 shows how the slope of the parabola in Figure 7 depends on the driving force for electron transfer. Although the *value* of the slope depends on the values of λ and $\Delta G_{k_{AB}^{(2)}}^0$, Marcus theory predicts that exothermic[48] reactions ($\Delta G_{k_{AB}^{(2)}}^0 < 0$) will have a slope less than $1/[2(\ln 10)k_BT]$, $(1/120 \text{ meV}^{-1}$ at $T = 300$ K), and endothermic reactions

(48) For electron transfer in RCs, the entropy term in the free energy is often neglected. We, therefore, use the term exothermic (endothermic) to refer to reactions in which the free energy is less than zero (greater than zero).

Table 2. Summary of Rate Equations for the Two-Step $k_{AB}^{(2)}$ Mechanisms[a]

	RATE LIMITING PROTON TRANSFER	RATE LIMITING ELECTRON TRANSFER
PROTON FIRST (upper path in fig. 3)	$\mathbf{k_{H+(1)}}$ MECHANISM 1	$f(\mathbf{Q_BH})\ \mathbf{k_e}$ MECHANISM 2
ELECTRON FIRST (lower path in fig. 3)	$f(\mathbf{Q_B^{2-}})\ \mathbf{k'_{H+(1)}}$ MECHANISM 3	$\mathbf{k'_e}$ MECHANISM 4

[a] Rate equations governing $k_{AB}^{(2)}$ under the simplifying conditions when one rate constant, either for electron transfer k_e (or k'_e) or for proton transfer $k_{H+(1)}$ (or $k'_{H+(1)}$), is much smaller than the other. $f(Q_BH^-)$ and $f(Q_B^{2-})$ denote the fraction of the intermediate states (see Figure 3).

($\Delta G_{k_{AB}^{(2)}}^0 > 0$) will have a slope greater than $1/[2(\ln 10)k_BT]$ $(1/120 \text{ meV}^{-1}$ at $T = 300$ K), regardless of the value of the reorganization energy.[49] These predictions of the Marcus theory have been experimentally verified and have been used to distinguish exothermic from endothermic electron transfers.[50,51] The observed slope of the free energy dependence will be used to discriminate between possible reaction mechanisms (see below).

Possible Mechanisms for Proton-Coupled Electron Transfer. Two models for the proton-coupled electron transfer are considered. (1) The first is the stepwise model. In this model proton and electron transfer are separate reaction steps; proton transfer can either precede or follow electron transfer as shown in Figure 3 to form a high-energy[52] intermediate state. When either proton transfer or electron transfer along a given path is the rate determining step, the proton-coupled electron transfer reaction can be modeled simply as one of four two-step mechanisms.[53] The rate equations that describe the overall process are summarized for the stepwise mechanisms in Table 2.

(2) The second is the concerted model. In this model proton transfer and electron transfer occur in one step and, in contrast to a stepwise model, no intermediate state is formed. At the transition state, the proton is partially transferred (or the solvent coordinate associated with proton transfer is polarized) such that following the instantaneous change in electron distribution due

(49) (a) Sutin, N. In *Inorganic Biochemistry*; Eichhorn, G. L., Ed.; Elsevier: Amsterdam, The Netherlands, **1973**; Vol. 2, pp 611−653. (b) Scandola, F.; Balzani, V.; Schuster, G. B. *J. Am. Chem. Soc.* **1981**, *103*, 2519−2523.

(50) (a) Klingler, R. J.; Kochi, J. K. *J. Am. Chem. Soc.* **1981**, *103*, 5839−5848. (b) Klingler, R. J.; Kochi, J. K. *J. Am. Chem. Soc.* **1982**, *104*, 4186−4196.

(51) Murphy, S. T.; Zou, C.; Miers, J. B.; Ballew, R. M.; Dlott, D. D.; Schuster, G. B. *J. Phys. Chem.* **1993**, *97*, 13152−13157.

(52) If either intermediate were lower in energy than the initial or final states then a fraction of this intermediate would be present at equilibrium, which is contrary to observation.[67] The lack of observation of these intermediates is not surprising in light of the energies required to protonate ($Q^- + H+ \rightarrow QH$) or to reduce ($Q^- + e^- \rightarrow Q^{2-}$) a semiquinone in solution. The energy required to protonate the semiquinone in aqueous solution at pH 7 is ~120 meV based on the pK value of 5 determined for Q_{10} in 80% ethanol.[74] The energy required to form doubly reduced Q^{2-} from Q^- in aprotic solvent has been measured to be 720 meV.[75]

(53) Although individual rates have not been measured, arguments based on experiment support the postulate that if the reaction occurs in a stepwise fashion then a single reaction step is rate determining. The free energy dependence is independent of pH (see Figure 6). This would not be expected if intrinsic rate constants (those determining which mechanism was dominant) were comparable at some pH. Instead, since the pH dependence of the intrinsic rate constants for electron and proton transfer are different,[12] a change in mechanism leading to a pH dependent free energy dependence would be expected. Additionally, the possibility of comparable values of the intrinsic electron and proton transfer rate constants is further ruled out for some cases by the observation of monoexponential decay kinetics for the $k_{AB}^{(2)}$ reaction. Biexponential kinetics will be observed in many situations when intrinsic rates are similar.

to electron transfer, the proton relaxes to a new equilibrium position bound to the semiquinone.

The predicted slopes of the free energy dependencies for each of the four stepwise mechanisms and the concerted mechanism are discussed below.

Mechanism 1. Upper Path in Figure 3 with $k_H \ll k_e$. Proton transfer precedes electron transfer and is rate limiting. A change in the intrinsic electron transfer rate due to quinone substitution will not be observable in the measurement of $k_{AB}^{(2)}$, i.e., $k_{AB}^{(2)} = k_H$. Since the observed rate is independent of the electron transfer rate, the predicted slope for this mechanism is zero.[54]

Mechanism 2. Upper Path in Figure 3 with $k_H \gg k_e$. Proton transfer precedes rate limiting electron transfer. This reaction scheme involves a pre-equilibrium between reactants and the protonated intermediate state. The rate constant $k_{AB}^{(2)}$ will be proportional to the fraction of protonated intermediate, $f(Q_BH)$, and the rate of electron transfer, k_e, i.e., $k_{AB}^{(2)} = f(Q_BH) \cdot k_e$. The mole fraction of the protonated intermediate in hybrid RCs is expected to be unchanged from that of native RCs. This fraction is given by

$$f(Q_BH) = \exp\{-[\Delta G_{H+}^0/kT]\} \qquad (9)$$

where ΔG_{H+}^0 is the free energy for protonation of Q_B^-. The intrinsic rate of electron transfer, k_e, is expected to change with the driving force according to eq 5. The slope of the free energy dependence is described by eq 8.

Mechanism 3. Lower Path in Figure 3 with $k'_H \ll k'_e$. Electron transfer precedes rate limiting proton transfer to Q_B^{2-}. The reaction mechanism predicts a pre-equilibrium between reactants and the intermediate state. The rate constant $k_{AB}^{(2)}$ will be proportional to the fraction of the secondary quinone dianion, $f(Q_B^{2-})$, and the rate of the proton transfer, k'_H, i.e., $k_{AB}^{(2)} = f(Q_B^{2-})k'_H$. No change in the rate constant k'_H is expected due to quinone substitutions made in this work. However, the rate of the observed reaction should be influenced by a change in the mole fraction of the secondary quinone dianion. This fraction is governed by the Boltzmann relation:

$$f(Q_B^{2-}) = \exp\{-(\Delta G_{(Mech. 3)}^0/k_BT)\} \qquad (10)$$

where $\Delta G_{(Mech. 3)}^0$ is the free energy between the initial, $Q_A^-Q_B^-$, and intermediate, $Q_AQ_B^{2-}$, states. The free energy dependence of the (relative) rate can be obtained from the rate equation, eqs 6 and 10. It is given by

$$\log \frac{k_{AB}^{(2)} hybrid}{k_{AB}^{(2)} native} = \frac{1}{\ln 10}\left[-\frac{\delta\Delta G^0}{k_BT}\right] \qquad (11)$$

The slope of the free energy dependence, obtained by taking the derivative of eq 11 with respect to $\delta\Delta G^0$, is $1/[(\ln 10)k_BT]$ (1/60 meV^{-1} at $T = 300$ K).

Mechanism 4. Lower Path in Figure 3 with $k'_H \gg k'_e$. Rate limiting electron transfer precedes protonation of the secondary quinone. The overall rate constant $k_{AB}^{(2)}$ for this

mechanism depends only on the intrinsic rate constant for electron transfer, k'_e, i.e. $k_{AB}^{(2)} = k'_e$. Similar to mechanism 2, eq 8 describes the slope of the free energy dependence predicted by the Marcus theory for mechanism 4. However, the *value* of the slope for mechanism 4 is expected to be different from that of mechanism 2 due to differences in the value of $\Delta G_{k_{AB}^{(2)}}^0$ for the two mechanisms (discussed below).

Mechanism 5. Middle Path in Figure 3. This represents a concerted proton and electron transfer. Quantitative models based on Marcus theory to describe the free energy dependence for electron transfer reactions concerted with bond breaking[31a] and concerted proton/proton transfer reactions[55] have been proposed. In accord with these models, the concerted proton-coupled electron transfer mechanism can be described using Marcus theory where the movement of the proton is treated as a special coordinate. The activation barrier to concerted electron and proton transfer is a function of the bonding energy of the proton, the reorganization energy associated with solvation of the proton donor/acceptor, and the solvent reorganization energy associated with electron transfer. Compared to a simple outer-sphere electron transfer reaction, the reorganization energy associated with a concerted reaction contains additional contributions. For this reason, the reorganization energy of mechanism 5 is expected to be larger than that of mechanisms 2 or 4. Since the free energy of the reaction $Q_A^-Q_B^- \rightarrow Q_AQ_BH^-$, $\Delta G_{eq}^0 = -70$ meV, is small, the slope of the free energy dependence should be close to $1/[2 \ln 10]k_BT$ (see eq 8).

Comparison of the Predictions of the Different Mechanisms with Experiment. Mechanisms 1 and 3. The measured dependence of the relative rate constant, $(k_{AB}^{(2)}hybrid/k_{AB}^{(2)}native)$, on the redox free energy (driving force) is shown on a semilogarithmic scale in Figure 8. The relative rate constant increases with increasing driving force, $\delta\Delta G^0$, by a factor of 10 per 160 meV, i.e. the slope is 1/160 meV^{-1}. The two mechanisms in which proton transfer is rate limiting (mechanisms 1 and 3) have slopes (shown in Figure 8) which disagree with the measured data. For mechanism 1, the slope is zero. For mechanism 3 the slope is 1/60 meV^{-1}. Thus, mechanisms 1 and 3 can be eliminated as possible mechanisms of the $k_{AB}^{(2)}$ reaction.

Mechanisms 2, 4, and 5. The slopes predicted for the mechanisms involving rate limiting electron transfer (mechanisms 2, 4, and 5) are dependent on the parameters (λ and $\Delta G_{k_{AB}^{(2)}}^0$) used in the model (see eq 8). Assuming reasonable values for these parameters allows comparison between theory and experimental observation. We expect λ for the $k_{AB}^{(2)}$ reaction to be similar to reorganization energies of other electron transfer reactions involving Q_B, since λ is likely to be dominated by fluctuations in the polar Q_B environment. Consequently, we will assume for mechanisms 2, 4, and 5[56] a value for λ of 1.1 eV as determined for the k_{BD} reaction ($D^+Q_AQ_B^- \rightarrow DQ_AQ_B$).[32] Differences in the predicted slopes for each mechanism stem from the differences in the driving force, $\Delta G_{k_{AB}^{(2)}}^0$. Estimates for the free energy of electron transfer for mechanisms 2, 4, and 5 (discussed in the Appendix) range between -150 and -310 meV, $+220$ and $+490$ meV, and -50 and -90 meV, respectively (see Figure 9). A range of theoretically predicted slopes for mechanisms 2, 4, and 5, calculated using eq 8 with $\lambda = 1.1$ eV and $\Delta G_{k_{AB}^{(2)}}^0$ in the ranges given, are shown as shaded regions in Figure 8. Mechanism 2 best fits the observed

(54) A rate limiting proton transfer reaction can, in principle, be tested by measuring the effect of deuterium isotope substitution on the observed rate. However, the results of deuteration can be ambiguous (Bell, R. P.; Goodall, D. M. *Proc. R. Soc. London, Ser. A.* **1966**, *294*, 273−297) especially in an RC system. For example, deuteration can have the effect of changing pK_as of acid groups including the pK_a of the protonated semiquinone. The quinone substitution technique described here should be able to determine unambiguously whether proton transfer is the rate limiting step (i.e., mechanism 1). In this mechanism, the slope of the free energy dependence would be zero.

(55) Albery, W. J. *Faraday Discuss. Chem. Soc.* **1982**, *74*, 245−256.
(56) In the concerted mechanism, motion along the proton coordinate contributes an additional term to the reorganization energy.[31a] Thus, 1.1 eV should be considered a lower limit for λ in mechanism 5.
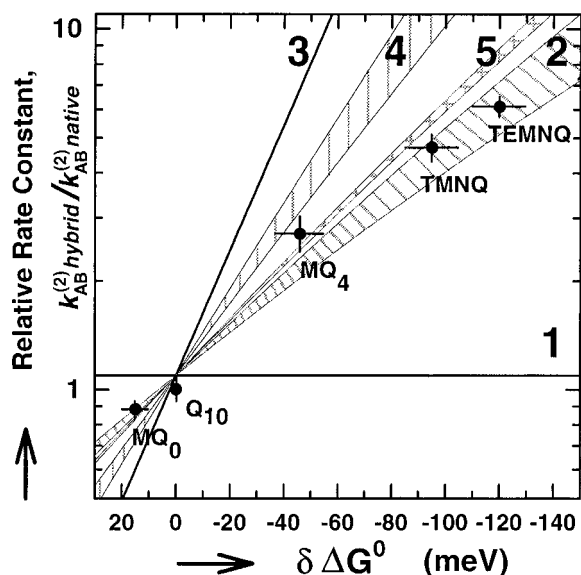
Figure 8. The relative rate constant of proton-coupled second electron transfer, ($k_{AB}^{(2)}$*hybrid*/$k_{AB}^{(2)}$*native*), as a function of the change in redox free energy (driving force) for electron transfer. Labeled curves and hatched areas represent the predicted dependencies of the possible mechanisms (see Figure 3). Curve 1: Rate limiting proton transfer preceding electron transfer (mechanism 1). Curve 3: Electron transfer preceding rate limiting proton transfer (mechanism 3). Area 2 (\\\): Reversible proton transfer preceding rate limiting electron transfer (mechanism 2). Area 4 (|||): Rate limiting electron transfer preceding proton transfer (mechanism 4). Area 5 (+): concerted electron and proton transfer. The data were taken from columns 5 and 7 of Table 1. Error bars represent the statistical deviation in the measured values. Quinones substituted into the Q_A site included the following: MQ_0, 2-methyl-1,4-naphthoquinone; MQ_4, 2-methyl-3-tetraisoprenyl-1,4-naphthoquinone; TMNQ, 2,3,5-trimethyl-1,4-naphthoquinone; and TEM-NQ, 2,3,6,7-tetramethyl-1,4-naphthoquinone.
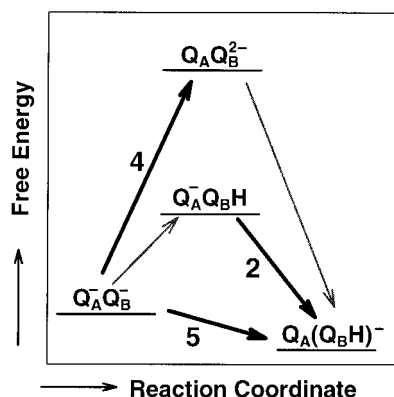
Figure 9. Relative energy levels of the states involved in the proton-coupled second electron transfer reaction (approximately to scale). The heavy arrows represent the rate limiting electron transfer steps of mechanisms 2, 4, and 5 with free energies denoted $\Delta G^0_{(Mech. 2)}$, $\Delta G^0_{(Mech. 4)}$, and ΔG^0_{eq}, respectively, in the text. The electron transfer steps of mechanisms 2 and 5 are exothermic while that for mechanism 4 is endothermic. Differences in the electron transfer driving force give rise to the differences in the predicted free energy dependencies for these mechanisms. The light arrow between states $Q_A^-Q_B^-$ and $Q_A^-Q_BH$ represents the proton transfer step of mechanism 2. The light arrow connecting states $Q_AQ_B^{2-}$ and $Q_A(Q_BH)^-$ represents the proton transfer step of mechanism 4.

data due to the large favorable free energy change predicted for this mechanism. The predicted slope for mechanism 4 (greater than $1/[2(\ln 10)k_BT]$) gives a much poorer fit to the data. The predicted slope for a concerted mechanism (close to $1/[2(\ln 10)k_BT]$) is only slightly poorer than for mechanism 2.

A larger λ for the concerted mechanism due to contributions from proton motion would worsen the fit.

The disagreement of the predictions for mechanisms 4 and 5 with experiment suggests that these mechanisms are less likely than mechanism 2. However, the relatively small discrepancy between these predictions and the observed slope does not provide sufficient grounds on which to unequivocally rule out mechanisms 4 or 5 since systematic changes to λ or T_{AB} can potentially alter the observed slope.[57] For this reason we discuss the results of kinetic experiments made in site directed mutant RCs which provide independent qualitative evidence that mechanism 4 can be excluded.

Predictions based on mechanism 4 are qualitatively inconsistent with observations made in site directed mutant RCs which change the redox potential of Q_B by changing the electrostatic environment around the Q_B binding site. As an example, consider the Asn-M44 → Asp replacement.[58] This mutation creates a more negative potential near Q_B, which is expected to destabilize (raise) the energy level of the $Q_AQ_B^{2-}$ intermediate state relative to $Q_A^-Q_B^-$. How is this expected to change $k_{AB}^{(2)}$ assuming that mechanism 4 shown in Figure 9 is operative? Decreasing the driving force for electron transfer between $Q_A^-Q_B^-$ and $Q_AQ_B^{2-}$ decreases the intrinsic electron transfer rate, k'_e, and, thus, $k_{AB}^{(2)}$. However, the rate constant, $k_{AB}^{(2)}$, was experimentally observed to **increase** in the Asn-M44 → Asp mutant[58] contrary to the prediction for mechanism 4. Moreover, for other mutant RCs with a more negative potential near Q_B, $k_{AB}^{(2)}$ was also increased[59] whereas in mutant RC with a more positive potential near Q_B, $k_{AB}^{(2)}$ was decreased.[15,59–61] These results are expected for mechanism 2 shown in Figure 9 and are explained by the changes in the free energy between the $Q_A^-Q_BH$ intermediate and the $Q_A^-Q_B^-$ initial state. The details of the concerted model are not sufficiently well defined to predict the change in $k_{AB}^{(2)}$ in the mutant RCs.

It has been suggested in a previous publication[20] that the $Q_AQ_B^{2-}$ intermediate state *could* be lower in energy than the $Q_A^-Q_BH$ intermediate and, therefore, mechanisms 3 or 4 was previously favored. However, the free energy dependence of $k_{AB}^{(2)}$, the observations made in mutant RCs described above, the estimates based on solution redox potentials, and other recent

(57) Some factors that may cause discrepancies between experiment and theory have been discussed by R. A. Marcus (*J. Phys. Chem.* **1968**, *72* (3), 891–899). In our case, the major contributor to the uncertainty in the observed slope arises from possible changes to λ and T_{AB} which may accompany quinone substitution. Although the assumption of a constant λ and T_{AB} is reasonable, based on the nearly identical structures of the quinones used in this work, we have not verified experimentally that λ and T_{AB} remain constant throughout the series of quinones and, therefore, cannot conclude unequivocally that the observed free energy dependence is different than expected for mechanisms 4 or 5. Discrepancies between experiment and the theoretical predictions of the Marcus theory can also arise if work terms (the work required to bring reactants together from an infinite separation to their separation distance in the reaction complex) are large or if there is a large asymmetry in the potential energy surfaces of reactants and products. These are, however, only minor contributors to the uncertainty in the reaction center system. The effect on the theoretical slope of even large asymmetries in the reactant and product potential energy surfaces is relatively small[47d] and work terms for electron transfer reactions in RCs are expected to be negligible since the redox centers are held at a constant separation by the protein matrix.

(58) Rongey, S. H.; Paddock, M. L.; Feher, G.; Okamura, M. Y. *Proc. Natl. Acad. Sci. U.S.A.* **1993**, *90*, 1325–1329.

(59) Paddock, M. L.; Feher, G.; Okamura, M. Y. *Biophys. J.* **1996**, *70*, A11.

(60) Paddock, M. L.; Feher, G.; Okamura, M. Y. *Biochemistry* **1995**, *34*, 15742–15750.

(61) In addition to these types of mutations there are mutations such as Asp L213 → Asn that result in a reaction which is rate limited by proton transfer. In these RCs $k_{AB}^{(2)}$ was found to be independent of driving force (mechanism 1).[69]

experimental results[15,62] argue otherwise. An assumption made in the previous analysis from which the pK_a of $(Q_BH)^-$ was estimated to be ~ 10.5 (below the solution value of ~ 14.5)[63] led to the low estimate for the $Q_AQ_B^{2-}$ energy and is now believed to be incorrect.[21,62]

We conclude that the free energy dependence of $k_{AB}^{(2)}$ rules out proton transfer as the rate limiting step and, therefore, eliminates mechanisms 1 and 3 (see Figure 3). The mechanism of rate limiting electron transfer followed by proton transfer (mechanism 4) is unlikely based on the free energy dependence of the rate as well as results from mutant RCs. The free energy dependence is consistent with a mechanism in which protonation of the semiquinone occurs prior to (mechanism 2) or concerted with electron transfer (mechanism 5). Although the best agreement with the observed free energy dependence is given by mechanism 2, the uncertainty in the fits to the observed dependence[57] precludes making a definitive choice between mechanisms 2 and 5. In these mechanisms, either complete or partial protonation of the semiquinone increases the driving force for electron transfer, leading to a faster rate. We call the process proton-activated electron transfer (PAET).

Either of the proposed mechanisms can readily account for the observed pH dependence of $k_{AB}^{(2)}$. In the two-step mechanism the pH dependence arises from the variation in the fraction of protonated semiquinone. In the concerted mechanism the pH dependence can arise from the fractional protonation of the proton donor to Q_B^-. Possible proton donors include the amino acid side chains of an electrostatically interacting cluster of residues near Q_B (e.g. Asp L213, Asp L210, Glu L212, and Glu H173).[64] Although these residues are not directly hydrogen bonded to the carbonyl oxygen of the quinone, protons may be transferred though an intervening H-bonded network of amino acid residues (including the hydroxyl group of Ser L223) and/or internal water molecules.[15,60,65,66]

Proposed Experiments to Distinguish between Mechanisms 2 and 5. Several experimental approaches can be used to distinguish between the concerted and the two-step mechanism 2. One approach is to detect the protonated semiquinone intermediate. The stepwise mechanism predicts an intermediate state, the presence of which should, in principle, be observable when the pH is reduced below the pK_a of Q_BH. Observation of the protonated semiquinone would provide compelling evidence for the stepwise PAET mechanism. Optical measurements in our lab down to pH 4 (below which RCs become unstable) have shown no evidence for changes in the typical

anionic semiquinone spectrum indicative of protonation.[67,68] It may be possible to extend the pH range by using different detergents or increase the pK of the semiquinone by using a different quinone or by changing the electrostatic environment around Q_B. Another approach is to observe the qualitative effect of deuterium isotope substitution. A k_{D_2O}/k_{H_2O} ratio above 1 would not be expected for a concerted process but could be explained by the two-step mechanism since deuteration should favor a larger fraction of the $Q_A^-Q_BH$ intermediate state. In contrast, a k_{D_2O}/k_{H_2O} ratio below 1 would not be expected for the two-step mechanism but could be explained by the concerted mechanism since deuteron transfer is involved in the rate limiting step of the reaction.

The Mechanism of Proton-Coupled Electron Transfer in Mutant RCs. Protonatable amino acids have been mutated to non-protonatable analogs to investigate the pathway(s) for proton transfer to Q_B in bacterial RCs (reviewed in refs 2 and 22). Site-directed mutants, *e.g.* Ser-L223 → Ala, Asp-L213 → Asn, Glu-H173 → Gln, show reductions in $k_{AB}^{(2)}$ ranging from 10^1- to 10^4-fold. The smaller values of $k_{AB}^{(2)}$ in these mutants have previously been attributed to a reduction in the rate of forward proton transfer to Q_B. However, alternate explanations can be advanced for the smaller $k_{AB}^{(2)}$, namely the mutation could reduce either the electron transfer rate, k_e (or k_{eH^+}), or the fraction of protonated intermediate state, $f(Q_BH)$. Hence, a smaller $k_{AB}^{(2)}$ is not sufficient to imply slow proton transfer to Q_B^-. The ambiguity in the interpretation of results can be removed using the quinone substitution experiment described in this work. If the mutation makes proton transfer rate limiting, then $k_{AB}^{(2)}$ will be independent of the electron driving force (mechanism 1). An observed rate constant, $k_{AB}^{(2)}$, independent of electron driving force was observed in Asp-L213 → Asn mutant RCs confirming that forward proton transfer is drastically slowed in this mutant.[69] It will be instructive to test other mutant RCs using this method to clarify the functional role of protein residues in proton and electron transfer to reduced Q_B.

The Mechanism of Proton-Coupled Electron Transfer in Other Systems. The protonation of electron acceptors (or deprotonation of electron donors) may play an important role in electron transfer processes of other biological systems. These include the following: other quinone proteins such as the cytochrome bc_1 complex,[70] flavoproteins such as ferrodoxin−NADP reductase,[71] the reduction of oxygen to water by cytochrome oxidase,[72] and the oxidation of water to oxygen by

(62) Recent results from studies of the titration of stigmatellin, a phenolic inhibitor of electron transfer which binds in the Q_B site, suggest that $pK_a(Q_BH^-)$ is $\gtrsim 2$ pK units higher when bound in the RC than when in solution (Graige, M. S.; Paddock, M. L.; Feher, G.; Okamura, M. Y. *Biophys. J.* **1996**, 70, A11). This result implies that $pK_a(Q_BH^-) \gtrsim 16$ and, thus, places the energy level of the $Q_AQ_B^{2-}$ intermediate state $\gtrsim 470$ meV above that of the initial state, consistent with the estimate of 490 meV based on solution redox potentials (see Appendix).

(63) Baxendale, J. H.; Hardy, H. R. *Trans. Faraday Soc.* **1953**, 49, 1140−1144.

(64) (a) Allen, J. P.; Feher, G.; Yeates, T. O.; Komiya, H.; Rees, D. C. *Proc. Natl. Acad. Sci. U.S.A.* **1988**, 85, 8487−8491. (b) Chirino, A. J.; Lous, E. J.; Huber, M.; Allen, J. P.; Schenck, C. C.; Paddock, M. L.; Feher, G.; Rees, D. C. *Biochemistry* **1994**, 33, 4584−4593.

(65) (a) Beroza, P.; Fredkin, D. R.; Okamura, M. Y.; Feher, G. In *The Photosynthetic Bacterial Reaction Center II*; Breton, J., Vermégleo, A., Eds.; Plenum Press: New York, 1992; pp 363−374. (b) Gunner, M. R.; Honig, B. *Proc. Natl. Acad. Sci. U.S.A.* **1991**, 88, 9151−9155.

(66) (a) Lancaster, C. R. D.; Ermler, U.; Michel, H. In *Anoxygenic Photosynthetic Bacteria*; Blankenship, R. E., Madigan, M. T., Bauer, C. E., Eds.; Kluwer Academic Publishers: Dordrecht, The Netherlands, 1995; pp 503−526. (b) Ermler, U.; Fritzsch, G.; Buchanan, S. K.; Michel, H. *Structure* **1994**, 2, 925−936. (c) Takahashi, E.; Wraight, C. A. *Proc. Natl. Acad. Sci. U.S.A.* **1996**, 93, 2640−2645.

(67) The intermediate states are not observed spectroscopically. The magnitude of semiquinone absorption measured at 450 nm in the RC indicates that following light excitation the quinone is in its anionic semiquinone form (i.e., the observed absorbance is equal to the extinction coefficient of Q_{10}^- multiplied by the RC concentration).[8] A smaller observed absorption would be expected if either intermediate state were present to any significant degree because the extinctions of Q_BH and Q_B^{2-} at 450 nm are much smaller than that of Q_B^- at 450 nm.[74,75]

(68) The fraction of the protonated intermediate state, Q_AQ_BH, was probed experimentally by measuring the amplitude of the semiquinone absorption in the reaction $DQ_AQ_B + DAD_{red.} \rightarrow DQ_AQ_B^- + DAD_{ox.}$ (*hv*) as a function of pH (this work). No decrease in the amplitude of semiquinone absorption between pH 8 and 4, indicative of a change in the protonation state of Q_B^-, was observed ($\pm 5\%$).

(69) Graige, M. S.; Paddock, M. L.; Feher, G.; Okamura, M. Y. *Biophys. J.* **1996**, 70, A11.

(70) Gennis, R. B.; Barquera, B.; Hacker, B.; Van Doren, S. R.; Arnaud, S.; Crofts, A. R.; DAvidson, E.; Gray, K. A.; Daldal, A. *J. Bioenerg. Biomembr.* **1993**, 25 (3), 195−209.

(71) Discussed in: *Falvins and Flavoproteins, 1987: Proceedings of the Ninth International Symposium*; Edmondson, D. E.; McCormick, D. B., Eds.; W. de Gruyten: Berlin, New York, 1987.

(72) Wikström, M. *Nature* **1989**, 338, 776−778.

photosystem II RCs.[73] The method of varying redox free energy to obtain the free energy dependence of a multi-step electron transfer reaction as described in this work may also be useful in investigating the mechanisms of proton-coupled electron transfer reactions in these and other systems.

Appendix

The free energy of electron transfer for mechanisms 2, 4, and 5 can be estimated from solution redox potentials, pK_as, and the measurement of the free energy difference between initial and final states made in RCs.[20] Knowledge of the free energies allows comparison between theoretical models and experimental observations and may be helpful in designing experiments to further differentiate between possible mechanisms.

$\mathbf{\Delta G^0_{eq}}$. The free energy for mechanism 5 (concerted reaction) is simply taken as the observed difference in free energy between the final and initial states. This energy gap ($\Delta G^0_{eq} = -70 \pm 20$ meV) has been measured in Glu-L212 → Gln mutant RCs[20] and is shown in Figure 9. The energy is assumed to be the same for native RCs since the mutation blocks only the delivery of the second proton to $(Q_BH)^-$, by forcing proton transfer to proceed through an alternate (unfavorable) proton transfer pathway, but does not change the thermodynamics of the $k^{(2)}_{AB}$ reaction.[13,20]

$\mathbf{\Delta G^0_{(Mech.\ 2)}}$. The free energy for the electron transfer of mechanism 2, $\Delta G^0_{(Mech.\ 2)}$, can be calculated from the free energy for protonation of Q_B^-, $\Delta G^0_{H_+}$, and the free energy of reaction, ΔG^0_{eq} (see Figure 9), as

$$\Delta G^0_{(Mech.\ 2)} = -\Delta G^0_{H_+} + \Delta G^0_{eq} \qquad (A1)$$

The lack of an observable fraction of protonated intermediate

sets a lower limit for $\Delta G^0_{H_+}$ of 80 meV[67,68] while a reasonable upper limit of 240 meV is set by the suggestion that the pK of Q_BH is greater than 3.[2,74] Using these estimates, $\Delta G^0_{(Mech.\ 2)}$ is between -150 and -310 meV.

$\mathbf{\Delta G^0_{(Mech.\ 4)}}$. The electron transfer reaction in mechanism 4 involves the oxidation of one quinone ($Q_A^- \rightarrow Q_A$) and the reduction of another ($Q_B^- \rightarrow Q_B^{2-}$). The free energy for this electron transfer, $\Delta G^0_{(Mech.\ 4)}$, can be estimated from the difference in the values for the redox couples (Q_{10}/Q_{10}^-) and (Q_{10}^-/Q_{10}^{2-}). The redox midpoint potential for the first electron reduction (pH 7) for ubiquinone in aqueous solution is -230 meV;[74] the redox midpoint potential for the second electron reduction of ubiquinone measured in aprotic solvent is -720 meV.[75] From the difference in these measured values the energy of the $Q_A Q_B^{2-}$ state is estimated to be $\sim$490 meV higher than the initial state. The value $\Delta G^0_{(Mech.\ 4)} = +490$ meV is used to define the upper boundry for mechanism 4 in Figure 8. The value of $+220$ meV, determined in a previous publication,[15] represents an experimentally determined lower limit for $\Delta G^0_{(Mech.\ 4)}$.

(73) Babcock, G. T.; Barry, B. A.; Debus, R. J.; Hoganson, C. W.; Atamian, M.; McIntosh, L.; Sithole, I.; Yocum, C. F. *Biochemistry* **1989**, *28* (25), 9557−9565.

(74) Swallow, A. J. In *Functions of Quinones in Energy Conserving Systems*; Trumpower, B. L., Ed.; Academic Press: New York, 1982; pp 59−72.

(75) Morrison, L. E.; Schelhorn, J. E.; Cotton, T. M.; Bering, C. L.; Loach, P. A. In *Functions of Quinones in Energy Conserving Systems*; Trumpower, B. L., Ed.; Academic Press: New York, 1982; pp 35−57.